

Electromagnetic wave propagation in alternating material-metamaterial layered structures

V.H. Carrera-Escobedo^a and H.C. Rosu^{b1}

¹IPICYT, Instituto Potosino de Investigación Científica y Tecnológica,
Camino a la presa San José 2055, Col. Lomas 4a Sección,
78216 San Luis Potosí, C.P. 78216, S.L.P., Mexico

Using the transfer matrix method we examine the parametric behavior of the transmittance of an electromagnetic plane wave propagating in the lossless regime through a periodic multilayered system as a function of the frequency and angle of incidence of the electromagnetic wave for the case in which the periodic structure comprises alternating material-metamaterial layers. A specific example of high transmittance at any angle of incidence in the visible region of the spectrum is identified.

I. INTRODUCTION

For a long time, *invisibility* has been a stimulating concept for science fiction novels and movies. In recent years, however, the scientific community has shown that this weird property can be achieved in principle in some “cloaking” devices through which plane waves propagate without inducing any kind of disturbances [1]. This type of devices can be fabricated by using *metamaterials*, which are engineered arrays of elements structured in such a way that the material is endowed with unusual and convenient properties for applications related to electromagnetic invisibility, [2–4]. Another attractive idea put forth by Alù and Engheta [5] is to use a shell of lossless plasmonic material or metamaterial to obtain transparency, originally at a single frequency, achieved through the strong reduction of the scattering cross section. Later, they also showed that multiple-frequency cloaking is possible if multilayered plasmonic shells are used to cover the dielectric or conducting object [6]. This multilayered coating idea for partial cloaking is currently pursued by many authors using in general plasmonic materials as examples [7, 8].

Here, we perform an investigation of planar multilayer structures with alternating material and metamaterial layers on which there is much less work, although in physical optics a common feature of planar periodic configurations is to generate transparency bands. Since we deal with a problem of wave propagation in a periodic structure we will use the transfer matrix method (TMM) to approach it. In the literature, one can find that the TMM is used to retrieve the electric permittivity ϵ and the magnetic permeability μ from the calculations of the scattering parameters [9]. Some time ago, Banerjee *et al* [10] calculated the intensity of the electromagnetic fields that propagate through an array of periodically alternating positive index media (PIM) and negative index media (NIM). However, they do not present their results in terms of either the angle of incidence or the frequency of the plane wave. They display the field intensity along the direction of propagation and compare the transfer matrix method to the finite element method concluding that the transfer matrix method provides the same results as the latter. Their results motivated us to use the transfer matrix method with the main goal of studying the effect of both the angle of incidence and frequency of the propagating plane wave on the transmittance spectrum as well as to see which parameters of the permittivity and the permeability might be convenient to achieve cloaking in such configurations. We compute the values of the transmittance for different values of ϵ and μ of the alternating material-metamaterial layers and search for convenient values that provide windows of transmittance for some regions of frequency as well as the complementary transmittance gaps that may be useful for making frequency filters [11].

II. THE TRANSFER MATRIX METHOD

A. Waves at an interface

To develop the TMM we must first know how the electromagnetic waves behave at the interface between two dielectrics. For plane waves at an interface, we consider that the electric and magnetic fields are given by

$$\vec{E} = \vec{E}_0 e^{i[\vec{k} \cdot \vec{r} - \omega t]} \quad (1)$$

$$\vec{H} = \vec{H}_0 e^{i[\vec{k} \cdot \vec{r} - \omega t]} , \quad (2)$$

^a victor.carrera@ipicyt.edu.mx

^b hcr@ipicyt.edu.mx

respectively. The two media in which the interface is in between will be characterized by permittivities ϵ_1 , ϵ_2 and permeabilities μ_1 , μ_2 , and the geometry of the wave vectors at the interface is illustrated in Fig. (1). In this figure, we assume that the wave is propagating along the z -axis and the two components of the wave vector are

$$\vec{k} = (k_x, 0, k_z) . \quad (3)$$

Because the condition of continuity of the tangential components of both the electric and magnetic fields

$$\vec{E}_{1t} = \vec{E}_{2t}, \quad \vec{H}_{1t} = \vec{H}_{2t} \quad (4)$$

must be satisfied for any point of the interface, the tangential components of \vec{k} have to be equal

$$k_{1x} = k_{2x} = k_x , \quad (5)$$

and using the dispersion relation $n^2\omega^2/c^2 = k^2$, then

$$\frac{n_1^2\omega^2}{c^2} = k_1^2 = k_x^2 + k_{1z}^2, \quad n_1 = \sqrt{\mu_1\epsilon_1} , \quad (6)$$

$$\frac{n_2^2\omega^2}{c^2} = k_2^2 = k_x^2 + k_{2z}^2, \quad n_2 = \sqrt{\mu_2\epsilon_2} , \quad (7)$$

for media 1 and 2, respectively. If k_x and k_z are real (that it is the case for planar waves), we can define the angles of incidence and refraction as

$$\tan \theta_1 = \frac{k_x}{k_{1z}} \quad (8)$$

and

$$\tan \theta_2 = \frac{k_x}{k_{2z}} , \quad (9)$$

respectively. From Eq. (5), we can see that

$$k_x = k_1 \sin \theta_1 = k_2 \sin \theta_2 \quad (10)$$

and if we apply the dispersion relationship we get

$$k_x = n_1 \frac{\omega}{c} \sin \theta_1 = n_2 \frac{\omega}{c} \sin \theta_2 . \quad (11)$$

If now we take the ratio of the last two equations we obtain *Snell's law*

$$\frac{\sin \theta_1}{\sin \theta_2} = \frac{n_2}{n_1} . \quad (12)$$

Considering the case of the TE polarization (type-s polarization), then \vec{E} is parallel to the interface, *i.e.*, we have

$$\vec{E} = (0, E, 0) \quad (13)$$

and

$$\vec{H} = (H_x, 0, H_z) . \quad (14)$$

We also have the boundary condition that says that the component of the electric field which is parallel to the interface is the same on both sides of the interfaces

$$E_1^+ + E_1^- = E_2^+ + E_2^- , \quad (15)$$

which holds for the magnetic field

$$H_{1x}^+ + H_{1x}^- = H_{2x}^+ + H_{2x}^- \quad (16)$$

as well as.

Using Maxwell's equation

$$\vec{k} \times \vec{E} = +\frac{\mu\omega}{c} \vec{H} , \quad (17)$$

in Eq. (16), we obtain

$$\frac{\mu_1\omega}{c} \vec{H}_{1x}^+ = -k_{1z} E_1^+ , \quad (18)$$

$$\frac{\mu_1\omega}{c} \vec{H}_{1x}^- = k_{1z} E_1^- . \quad (19)$$

Inserting (18) in (16) one can obtain

$$-\frac{k_{1z}c}{\mu_1\omega} E_1^+ + \frac{k_{1z}c}{\mu_1\omega} E_1^- = -\frac{k_{2z}c}{\mu_2\omega} E_2^+ + \frac{k_{2z}c}{\mu_2\omega} E_2^- . \quad (20)$$

Now we can write Eqs. (20) and (15) as

$$\begin{pmatrix} 1 & 1 \\ -\frac{k_{1z}}{\mu_1} & \frac{k_{1z}}{\mu_1} \end{pmatrix} \begin{pmatrix} E_1^+ \\ E_1^- \end{pmatrix} = \begin{pmatrix} 1 & 1 \\ -\frac{k_{2z}}{\mu_2} & \frac{k_{2z}}{\mu_2} \end{pmatrix} \begin{pmatrix} E_2^+ \\ E_2^- \end{pmatrix} \quad (21)$$

or

$$\begin{pmatrix} E_2^+ \\ E_2^- \end{pmatrix} = \mathbf{M}^{(s)} \begin{pmatrix} E_1^+ \\ E_1^- \end{pmatrix} \quad (22)$$

where

$$\mathbf{M}^{(s)} = \frac{1}{2} \begin{pmatrix} 1 + \frac{\mu_2 k_{1z}}{\mu_1 k_{2z}} & 1 - \frac{\mu_2 k_{1z}}{\mu_1 k_{2z}} \\ 1 - \frac{\mu_2 k_{1z}}{\mu_1 k_{2z}} & 1 + \frac{\mu_2 k_{1z}}{\mu_1 k_{2z}} \end{pmatrix} . \quad (23)$$

By a similar procedure, we can obtain the expression of the transfer matrix for the case of TM polarization (type-p)

$$\begin{pmatrix} E_2^+ \\ E_2^- \end{pmatrix} = \mathbf{M}^{(p)} \begin{pmatrix} E_1^+ \\ E_1^- \end{pmatrix} \quad (24)$$

$$\mathbf{M}^{(p)} = \frac{1}{2} \begin{pmatrix} 1 + \frac{\epsilon_2 k_{1z}}{\epsilon_1 k_{2z}} & 1 - \frac{\epsilon_2 k_{1z}}{\epsilon_1 k_{2z}} \\ 1 - \frac{\epsilon_2 k_{1z}}{\epsilon_1 k_{2z}} & 1 + \frac{\epsilon_2 k_{1z}}{\epsilon_1 k_{2z}} \end{pmatrix} . \quad (25)$$

For materials with only real dielectric constants we can express the wave vectors as

$$k_{1z} = k_1 \cos \theta_1 \quad \text{and} \quad k_{2z} = k_2 \cos \theta_2 , \quad (26)$$

so the transfer matrices for the TE and TM cases are written as

$$\mathbf{M}^{(s \text{ or } p)} = \frac{1}{2} \begin{pmatrix} 1 + z_{21} \frac{\cos \theta_1}{\cos \theta_2} & 1 - z_{21} \frac{\cos \theta_1}{\cos \theta_2} \\ 1 - z_{21} \frac{\cos \theta_1}{\cos \theta_2} & 1 + z_{21} \frac{\cos \theta_1}{\cos \theta_2} \end{pmatrix} , \quad (27)$$

where $z_{21} = \mu_2 k_1 / \mu_1 k_2$ for the s-polarization and $z_{21} = \epsilon_2 k_1 / \epsilon_1 k_2$ for the p-polarization.

B. Waves propagating through a slab

For a set of interfaces, the system behaves as a slab (like a sandwich of media). A simple example is given in Fig. (2). For such systems, it is enough to apply the composition law for transfer matrices [12]. In this way, the relationship of the coefficients of entry and exit is given by

$$\begin{pmatrix} E_3^+ \\ E_3^- \end{pmatrix} = \mathbf{M}^{12} \begin{pmatrix} e^{ik_{2z}\ell} & 0 \\ 0 & e^{-ik_{2z}\ell} \end{pmatrix} \mathbf{M}^{23} \begin{pmatrix} E_1^+ \\ E_1^- \end{pmatrix} , \quad (28)$$

where ℓ is the length of the slab in the direction of propagation.

From the last equation, one can obtain the transfer matrix for the slab as

$$\mathbf{M}_{\text{slab}}^s = \mathbf{M}^{12} \begin{pmatrix} e^{ik_{2z}\ell} & 0 \\ 0 & e^{-ik_{2z}\ell} \end{pmatrix} \mathbf{M}^{23} ,$$

which can be used for the generalization to the multilayer case.

Parameter	Value
ϵ_0	1.0
ϵ_+	2.0
ϵ_-	-1.0
μ_0	1.2
μ_+	2.0
μ_-	-1.2
n_b	2,3,5

TABLE I: The values of the permeabilities and permittivities of the AB slabs used for the case of a variable number of blocks.

C. Wave propagation through a multilayered system

The next step is to consider a multilayered system as illustrated in Fig. (3). For a system of this class, the transfer matrix is obtained by applying the composition law again. In this way, we have an *interface* matrix $\mathbf{M}^{i,i+1}$ for every interface and a *propagation* matrix of the form

$$\mathbf{P} = \begin{pmatrix} e^{ik_2 z \ell} & 0 \\ 0 & e^{-ik_2 z \ell} \end{pmatrix} \quad (29)$$

for every slab in which the electromagnetic wave propagates. In this manner, for a ten multilayer slab system (5 *A* and 5 *B* layers) the transfer matrix is written as

$$\mathbf{M} = M_{0A} [P_A M_{AB} P_B M_{BA}]^4 P_A M_{AB} P_B M_{B0} \quad (30)$$

where M_{0X} is the interface matrix between air and medium X , P_X is the propagation matrix of medium X , and M_{XY} is the interface matrix between medium X and medium Y . The \mathbf{M} and M_{XY} matrices are transfer matrices for the s-polarization or the p-polarization, depending on the nature of the incident wave.

Once the transfer matrix for the multilayered system has been obtained, one can proceed with the calculation of the transmission amplitude based on its definition for the case of electromagnetic waves given by [12]

$$t = \frac{\det \mathbf{M}}{\mathbf{M}_{22}} , \quad (31)$$

and the transmittance as its square modulus

$$T = |t|^2 . \quad (32)$$

III. NUMERICAL SIMULATIONS

The computation of the transmission amplitude is made by using a simple code written on python [13]. The system which we model has up to ten slabs, alternating a PIM with a NIM. The PIM is characterized by μ_+ and ϵ_+ , while the NIM is characterized by μ_- and ϵ_- . The frequency of the incident wave is in $c/(\ell\sqrt{\epsilon_0})$ units, where the chosen numerical value for ℓ is $1.0 \text{ }\mu\text{m}$, and the angle of incidence θ goes from $-\pi/2 < \theta < \pi/2$ which we normalize to $\theta_0 = \pi/2$ in the figures. The plots of transmission versus frequency are obtained for an angle of incidence of $\pi/3$. The range of frequencies goes from 300 THz to 1200 THz, which entails the frequency band of the visible light (430-770 THz). In the units of the plots, the band of frequencies of the visible light is [1.4-2.5] and is indicated by two horizontal black solid lines in the contour figures.

A. The effect of the number of layers

We begin by analyzing the effect of the number of layers upon the transmission spectrum. With this task in mind, we vary the number of periods “AB” crossed by the propagating wave using the values of the parameters given in Table I, where the parameters ϵ_0 and μ_0 correspond to the respective values for the relative permittivity and permeability of the medium (usually air) in front and at the end of the “AB” multilayer structure. We call the “AB” period a block. In Fig. (7), the number of blocks is increased from two to five, (in terms of interfaces, from

Parameter	Value
ϵ_0	1.0
ϵ_+	1.5, 2.0, 3.0
ϵ_-	-1.5, -2.0, -3.0
μ_0	1.2
μ_+	2.0
μ_-	-1.2
n_b	3

TABLE II: The values of the permeability and permittivity used when the number of blocks is kept fixed.

five to eleven), and each panel is labeled by the corresponding number of blocks. The regions of high transmittance show up as three symmetrical bubbles. Upon increasing the number of blocks in the system, one can see that the number of peaks inside each of the bubbles increases, and the number of peaks, n_{peaks} , is equal to twice the number of blocks, n_b , minus one, $n_{peaks} = 2n_b - 1$. This might be seen alike to the case of quantum systems if the number of quantum wells is put in correspondence with the number of peaks in the transmittance. One can also see that when the number of blocks increases the transmittance between the bubbles of high transmittance becomes smaller. This is a consequence of the change in the transmittance values that one can see in Fig. (4), where we can also notice that the transmittance bands get wider as the number of blocks increases. Moreover, in Fig. (7), we can see that we have a bubble of high transmittance inside the limits of the visible frequencies (black horizontal lines), which could be useful for cloaking devices. In addition, as we increase the number of blocks, this high transmittance region entails a wider range of angular values. On the other hand, if we increase the number of blocks enough the simulation ends up in a completely opaque material with zero transmittance as expected.

B. The effect of ϵ_+ and ϵ_-

Knowing that the number of blocks gives place to a series of transmittance bands, one naturally may ask if there is a way to control the width of these bands by means of the electric permittivities of the slabs. The values of the parameters that we use for this computation are given in Table II.

The results are presented in Fig. (8). We can see that the effect of increasing ϵ_+ while keeping ϵ_- fixed at -1.0 , is to tighten the bubbles of high transmittance, and the magnitude of this effect is proportional to the increase in ϵ_+ . When ϵ_+ is high enough, the bubbles lose the connection between them and become independent ovals. For this case, we see that the effect is similar for both the TE and TM modes, but for the TM mode the bubbles are more separated and there appears a series of smaller bubbles of high transmittance. Moreover, for both types of modes there is a shift to lower frequencies of these bubbles of high transmittance. This can be seen in the left panel of Fig. (5).

On the other hand, if we increase the value of $|\epsilon_-|$ while keeping ϵ_+ fixed at 2.0 we can see from Fig. (9) that the bubbles of high transmittance are absent and in their place a wide band with horizontal spikes occurs. Therefore, we conclude that the bubbles stem from the values of ϵ_+ . When ϵ_- increases, we can see that the wide band is fragmented in three sections, and the separation between sections is proportional to the increment in $|\epsilon_-|$. In this case, there is no shift to lower frequencies. This fact can be observed in the right panel of Fig. (5). The effect is similar for both TE and TM modes, but in the TM case the decrease in transmittance is less but in a wider range of frequencies.

In general, we can say that the value of ϵ_+ determines the form of the transmittance bands and the frequency range where they appear. On the other hand, the value of ϵ_- determine the width of the horizontal transmittance spikes.

C. The effect of μ_+ and μ_-

Now we study the effects of increasing the values of the permeabilities of the system. For this end, we use the values from Table III for the parameters that we can control.

From Fig. (10), we see that if we increase the magnitude of μ_+ the bubbles of high transmittance have a shift to lower frequencies which is proportional to the magnitude of μ_+ . Unlike the case of variable ϵ_+ , we see that the bubbles remain connected, and as the value of μ_+ increases the contact area between bubbles increases as well as. This is opposite to the case of variable ϵ_+ and occurs for both the TE and TM modes.

From the left panel of Fig. (6), we can appreciate easily a shifting effect to lower frequencies. Also, and even more interesting, we see that if we increase the value of μ_+ the valleys (regions of low transmittance) become less apparent. Thus, increasing μ_+ has the effect of rising the valleys of transmittance diminishing the relative borders of the transmittance bands.

Parameter	Value
ϵ_0	1.0
ϵ_+	2.0
ϵ_-	-1.0
μ_0	1.2
μ_+	1.5, 2.0, 3.0
μ_-	-1.5, 2.0, 3.0
n_b	5

TABLE III: The parameters used when the μ values are changed.

In the case of increasing the values of $|\mu_-|$, Fig. (11) shows that the main effect is to diminish the transmittance between the three regions of high transmittance. This effect is also visible on both the TE and TM modes. However, in this case, we notice that there is no shifting effect, which can be seen easily from the right panel of Fig. (6).

In addition, Figs. (7) - (11) show that the regions of high transmittance do not vary with the angle of incidence, which may be related to the independence of the polarization angle of the incident wave as also reported in [14]. Considering that the reflectance and transmittance are complementary properties, our findings regarding the transmittance spectrum seem to be in agreement with those reported in [15] for an Ag-TiO₂ multilayer system, which is the standard multilayer candidate with high transmittance in the visible region.

IV. CONCLUSION

We have obtained the transmission properties of a multilayered structure of alternating positive index media and negative index media using the TMM. The results of this study show that we can use the magnetic permeability and electric permittivity of such a system to create a profile of transmittance that fits some cloaking requirements. In particular, we have sought here for profiles of high transmittance at any angle of incidence in the visible region of the spectrum. In this respect, our results suggest a system with the properties displayed in Fig. (7), i.e., with $\epsilon_+ = 2.0$, $\epsilon_- = -1.0$, $\mu_+ = 2.0$, and $\mu_- = -1.2$, for the case of five blocks, $n_b = 5$, which present an almost uniform region of high transmittance in the visible part of the electromagnetic spectrum.

In addition, we have studied the manner in which the permeability and permittivity parameters affect the transmission properties in an alternation of material and metamaterial. We have observed that positive permeabilities may have the effect of reversing the appearance of the transmission bands that one may see in multilayered structures. On the contrary, positive permittivities have the effect of making the transmittance bands more pronounced. Somewhat surprisingly, the negative values of the electromagnetic material parameters do not have relevant effects in these settings.

ACKNOWLEDGMENTS

The first author acknowledges the financial support of CONACyT through a doctoral fellowship at IPICyT.

REFERENCES

- [1] P. Alitalo and S. Tretyakov, Electromagnetic cloaking with metamaterials, *Materials Today* **12**, 22-29 (2009).
- [2] J.B. Pendry, D. Schurig, and D.R. Smith, Controlling electromagnetic fields, *Science* **312**, 1780-1782 (2006).
- [3] T. Ergin, N. Stenger, P. Brenner, J.B. Pendry, and M. Wegener, Three-dimensional invisibility cloak at optical wavelengths, *Science* **328**, 337-339 (2010).
- [4] Q. Cheng, T.J. Cui, W.X. Jiang, and B.G. Cai, An omnidirectional electromagnetic absorber made of metamaterials, *New J. Phys.* **12**, 063006 (2010).
- [5] A. Alù and N. Engheta, Achieving transparency with plasmonic and metamaterial coatings, *Phys. Rev. E* **72**, 016623 (2005).

- [6] A. Alù and N. Engheta, Multifrequency optical invisibility cloak with layered plasmonic shells, *Phys. Rev. Lett.* **100**, 113901 (2008).
- [7] K.-H. Kim, Y.-S. No, S. Chang, J.-H. Choi, and H.-G. Park, Invisible hyperbolic metamaterial nanotube at visible frequency, *Sci. Rep.* **5**, 16027 (2015).
- [8] C. Díaz-Aviño, M. Naserpour, C.J. Zapata-Rodríguez, Conditions for achieving invisibility of hyperbolic multilayered nanotubes, *Opt. Commun.* **381**, 234-239 (2016).
- [9] D.R. Smith, D. C. Vier, Th. Koschny, and C. M. Soukoulis, Electromagnetic parameter retrieval from inhomogeneous metamaterials, *Phys. Rev. E* **71**, 036617 (2005).
- [10] P.P. Banerjee, H. Li, R. Aylo, and G. Nehmetallah, Transfer matrix approach to propagation of angular plane wave spectra through metamaterial multilayer structures, *Proc. SPIE* **8093**, 3387-3389 (2011).
- [11] L. Solymar and E. Shamonina, *Waves in Metamaterials* (Oxford University Press, Oxford, 2009).
- [12] P. Markoš and C.M. Soukoulis, *Wave propagation, from electrons to photonic crystals and left-handed materials* (Princeton University Press, Princeton and Oxford, 2008).
- [13] Python Software Foundation. Python Language Reference, version 2.7. Available at <http://www.python.org>
- [14] B.-X. Wang, Single-patterned metamaterial structure enabling multi-band perfect absorption, *Plasmonics* DOI:10.1007/s11468-016-0234-1 (2016).
- [15] P. Shekhar, J. Atkinson, and Z. Jacob, Hyperbolic metamaterials: fundamentals and applications, *Nano Convergence* **1:14** (2014).

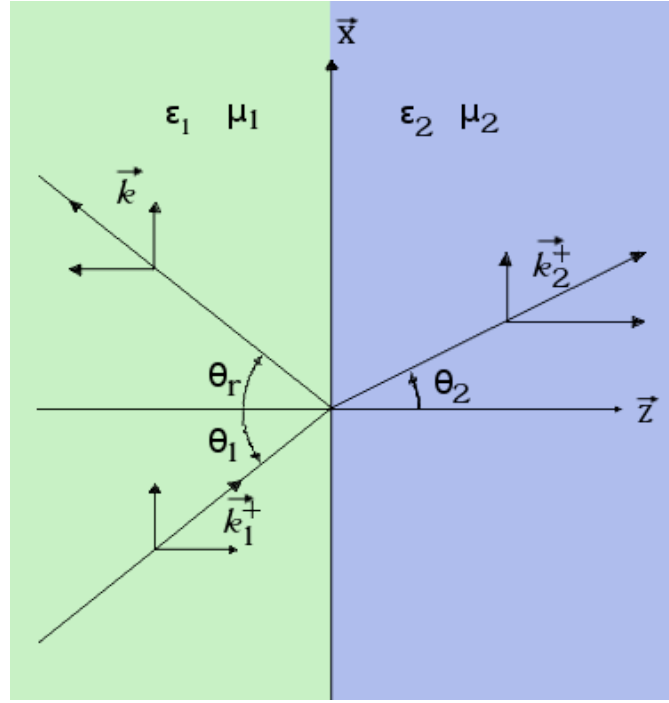


FIG. 1: Electromagnetic wave vectors at the interface between two different media.

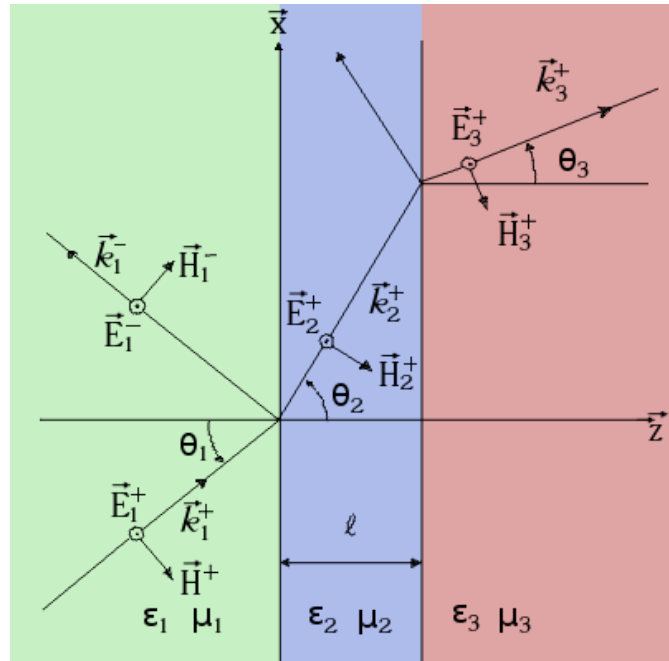


FIG. 2: Illustration of wave propagation through a slab composed of three different media.

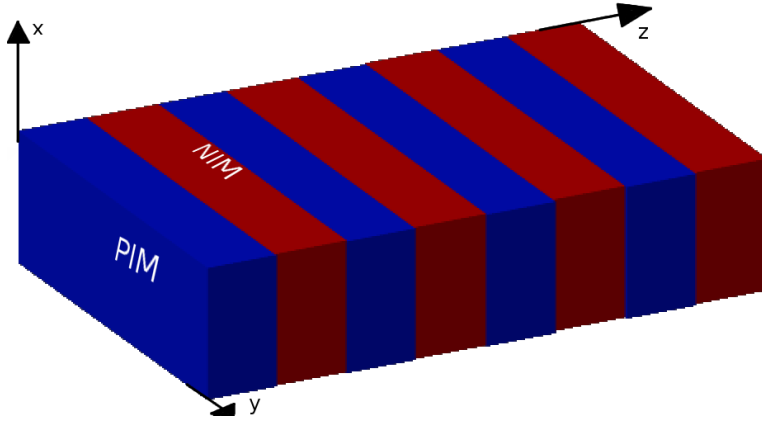


FIG. 3: A system formed by two types of slabs. The first one is a PIM (blue) labeled as *A* in the text, and the second is a NIM (red) labeled as *B* in the text.

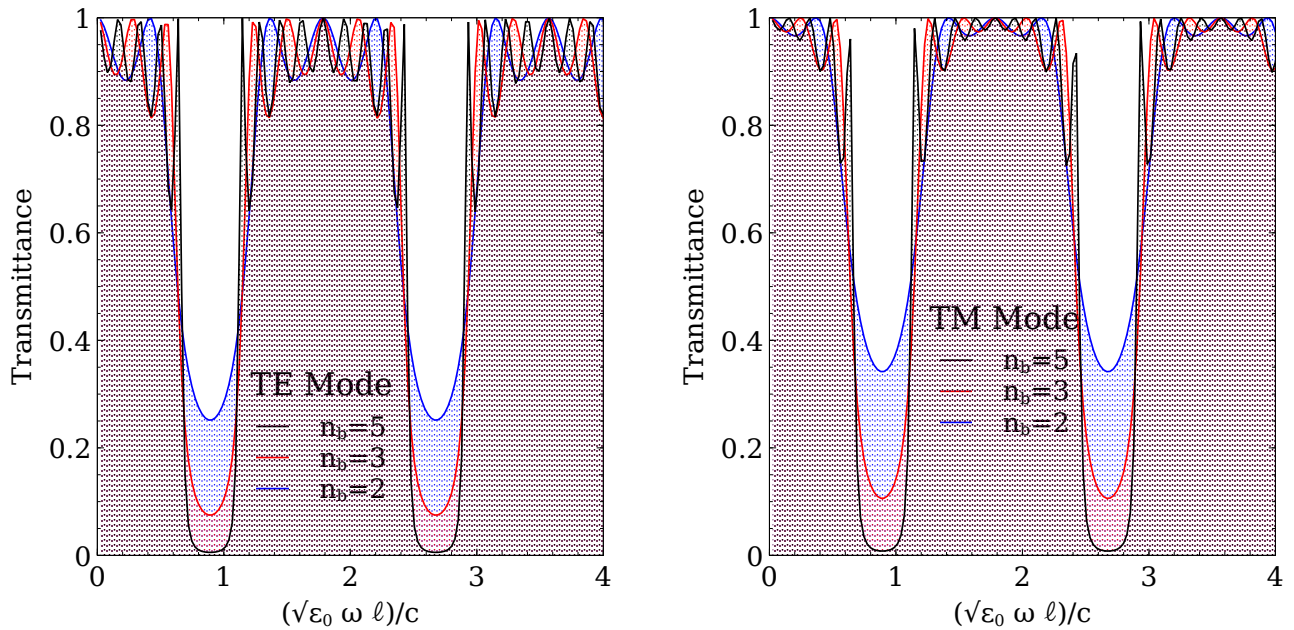


FIG. 4: Plots corresponding to the case of variable number of blocks. Left panel: the TE mode. Right panel: the TM mode. In these graphs we can see that the valleys of the transmittance get deeper as we increase the number of blocks. This is congruent with the formation of transmission bands in the case of superlattices.

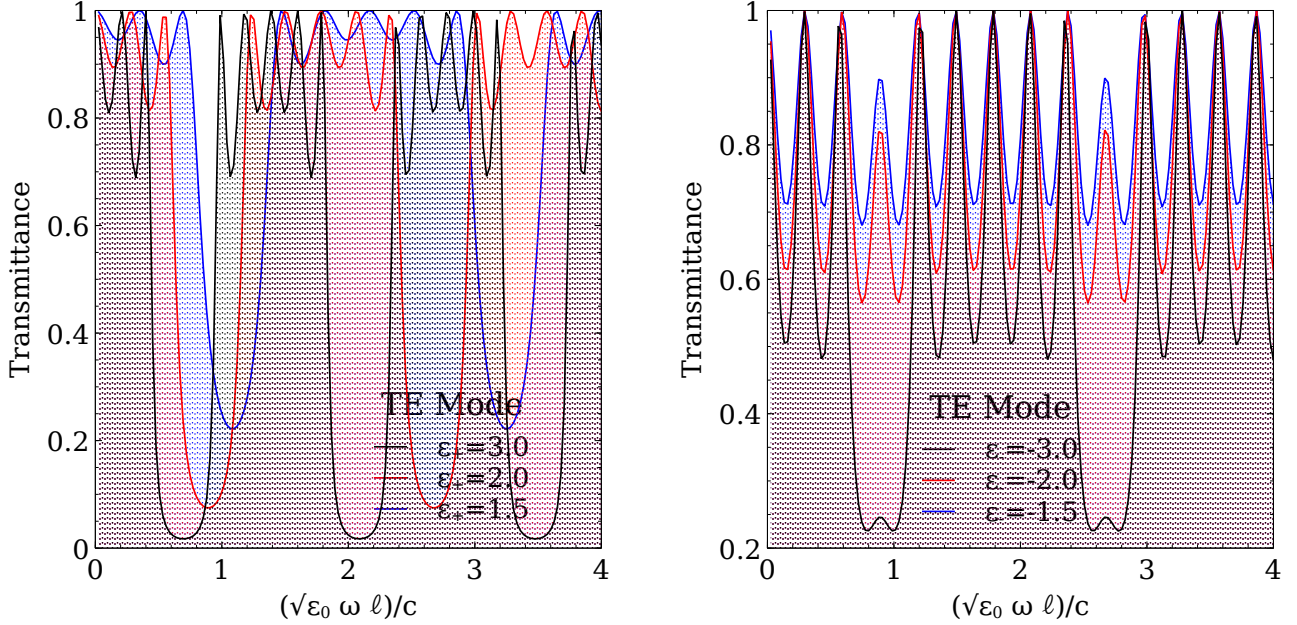


FIG. 5: Plots corresponding to the case of fixed angle of incidence $\theta = \pi/3$. The left panel corresponds to the case of variable ϵ_+ and the right panel corresponds to the case of variable ϵ_- . In these graphs, we can see the shifting of the peaks in transmittance only for the case with increasing ϵ_+ .

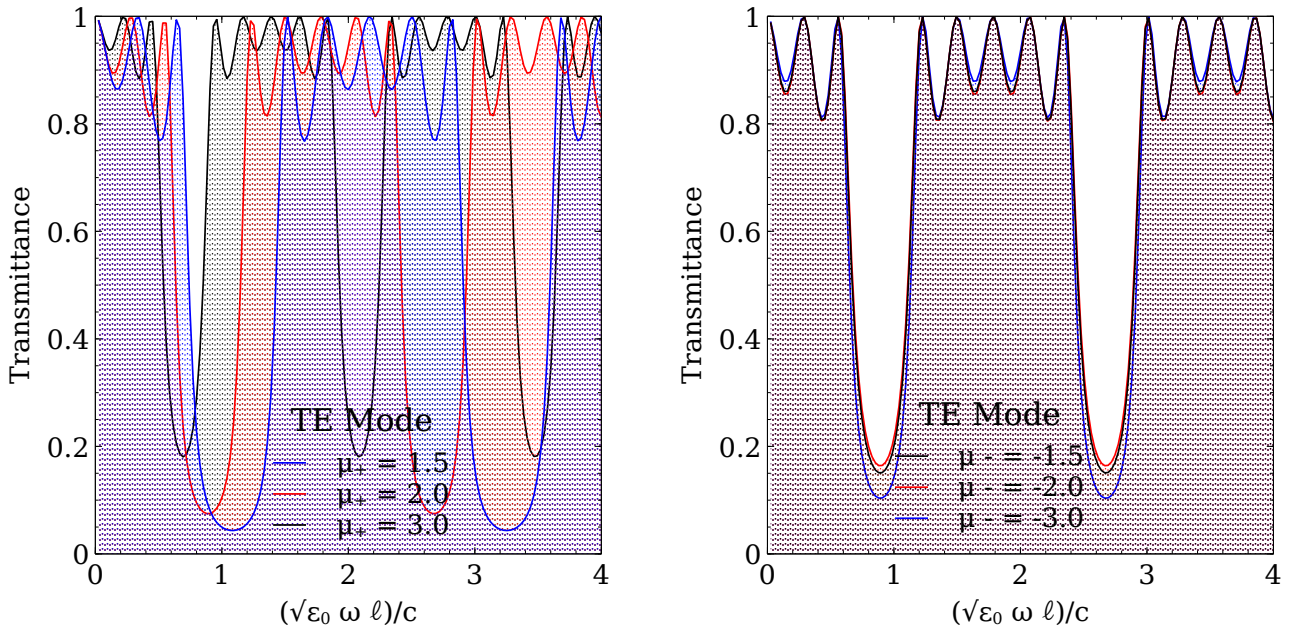


FIG. 6: Plots corresponding to the case of fixed angle of incidence $\theta = \pi/3$. Left panel: case of variable μ_+ . Right panel: case of variable μ_- . One can see that the shifting of the peaks in transmittance occurs only upon increasing μ_+ (left panel) and there is no shifting effect when $|\mu_-|$ is increased (right panel).

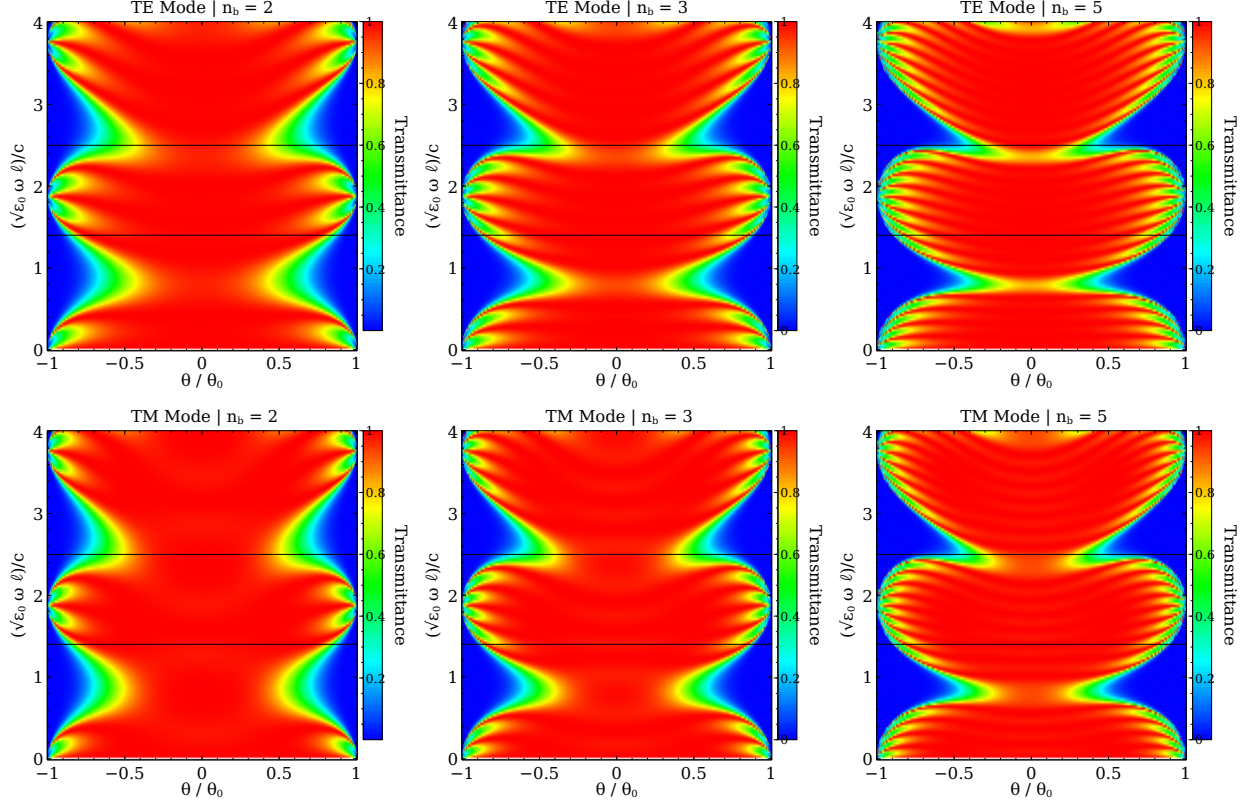


FIG. 7: Contour plots of the transmittance. The top row corresponds to the TE mode (s-wave) while the bottom row corresponds to the TM mode (p-wave). The x -axis corresponds to the angle of incidence, the y -axis to the frequency of incidence scaled by $\ell\sqrt{\epsilon_0}/c$, and the color bars correspond to transmittance. The black horizontal lines indicate the limits of the visible spectrum.

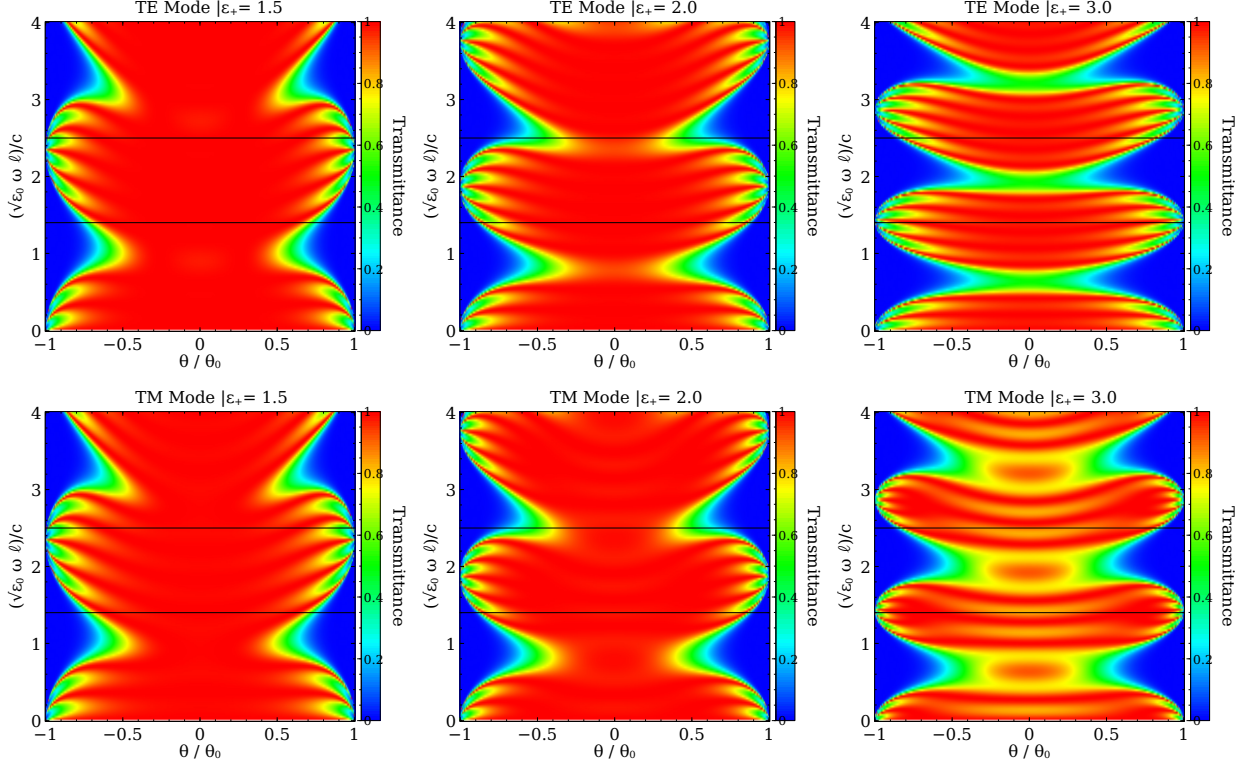


FIG. 8: Contour plots of the transmittance. The top row corresponds to the TE mode while the bottom row corresponds to the TM mode for three values ϵ_+ with ϵ_- fixed at -1.0, $\mu_+ = 2.0$, and $\mu_- = -1.2$.

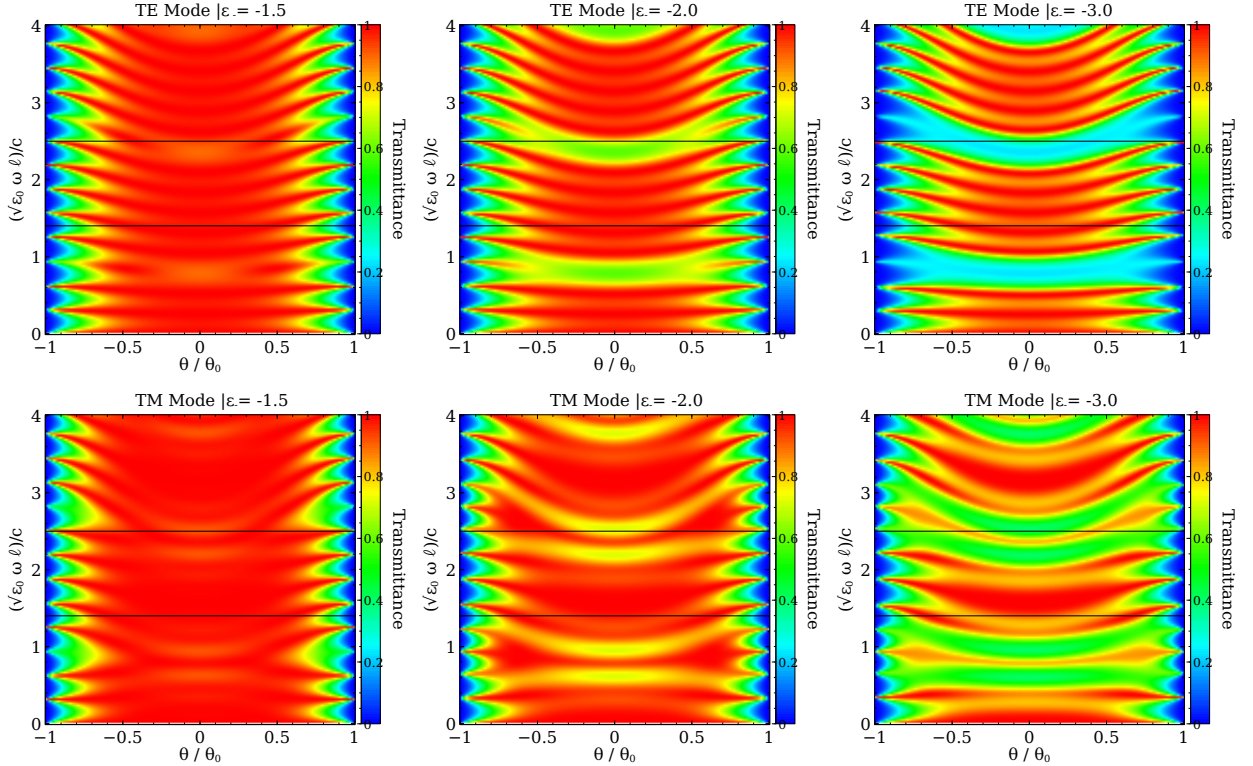


FIG. 9: Same as in the previous figure, but with the negative permittivity taking the values $|\epsilon_-| = 1.5, 2, 3$ while ϵ_+ is fixed at 2.0, $\mu_+ = 2.0$, and $\mu_- = -1.2$.

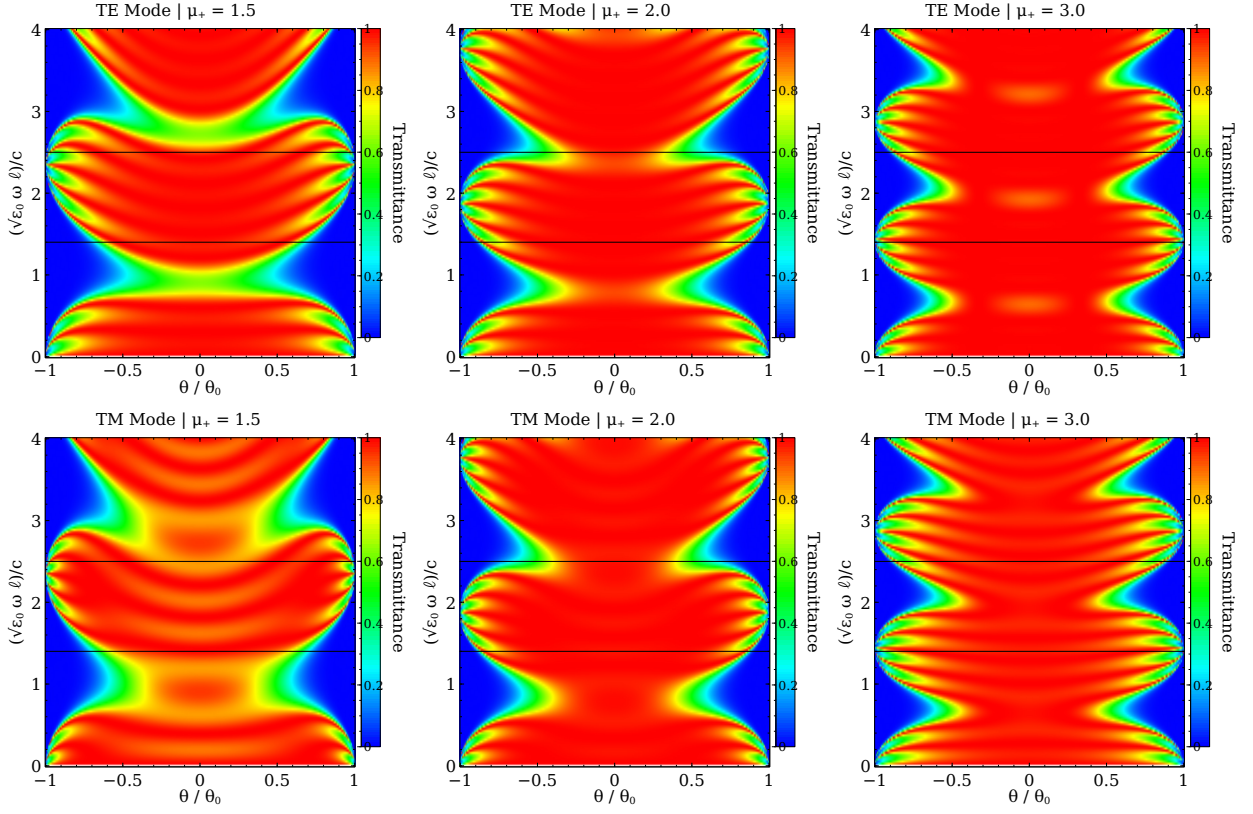


FIG. 10: Same as previously but for various μ_+ while μ_- kept fixed at -1.2, $\epsilon_+ = 2.0$, and $\epsilon_- = -1.0$.

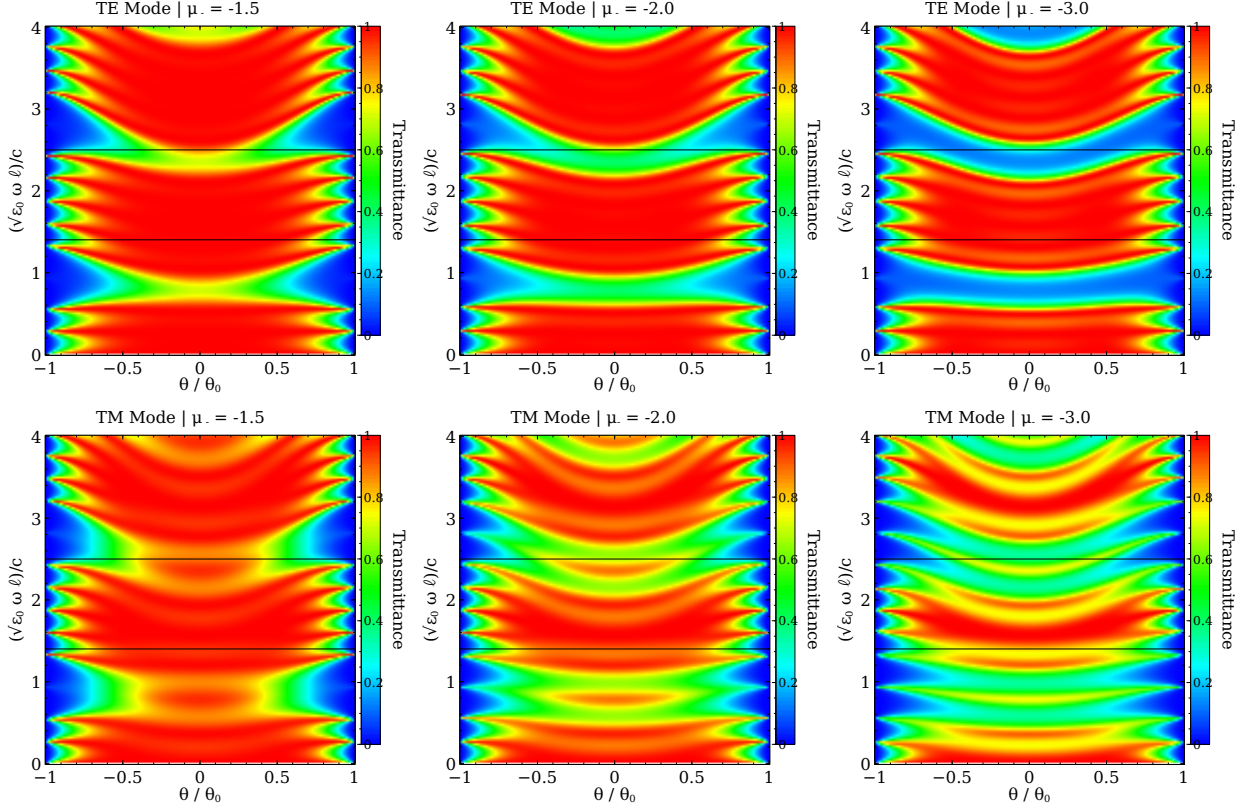


FIG. 11: Same as previously but for various μ_- and μ_+ kept fixed at 1.2, $\epsilon_+ = 2.0$, and $\epsilon_- = -1.0$.